

Computations of diffusivities in ice and CO₂ clathrate hydrates via molecular dynamics and Monte Carlo simulations

Alexander Demurov, Ravi Radhakrishnan, and Bernhardt L. Trout^{a)}

Chemical Engineering Department, Massachusetts Institute of Technology, Cambridge, Massachusetts 02139

(Received 21 June 2001; accepted 15 October 2001)

We report molecular simulation studies of the diffusion processes in ice and CO₂ clathrate hydrates performed using classical potential models of water (SPC/E) and carbon dioxide (EPM2). The diffusivity of H₂O in ice is calculated to be $1.3 \times 10^{-18} \text{ m}^2 \text{ s}^{-1}$ at 200 K using molecular dynamics simulations, a result in good agreement with experimental data. We also computed the diffusivity of H₂O and CO₂ in clathrate hydrates using both molecular dynamics and Monte Carlo simulations together with the Landau free energy method. We calculated free energy barriers for the CO₂ hopping between clathrate cages with and without a water defect present. We determined that a water vacancy was necessary for diffusion of CO₂, and we estimated the diffusion coefficient of CO₂ molecules in clathrate hydrates to be $1 \times 10^{-12} \text{ m}^2 \text{ s}^{-1}$ at 273 K and H₂O in the clathrate hydrates to be $1 \times 10^{-23} \text{ m}^2 \text{ s}^{-1}$ at 200 K. © 2002 American Institute of Physics.
[DOI: 10.1063/1.1425821]

I. INTRODUCTION

The computation of the mechanisms and rates of diffusion in solid materials is both a great need and a great challenge in chemical physics. In this study we use molecular simulations in order to meet this need for ice and CO₂ clathrate hydrates. Our objectives are (1) to validate our potentials and methods on ice, for which the mechanism and rate of diffusion are established,^{1–4} (2) to compute the diffusivity of both CO₂ and H₂O in clathrate hydrates, and (3) to enhance the understanding of diffusion in solid materials.

Clathrate hydrates are crystalline structures formed by hydrogen bonded water molecules. The framework of these structures consists of distinct cages, a fraction of which contain guest molecules, such as carbon dioxide.⁵ These materials are important in the injection of liquid carbon dioxide at depths greater than 500 m, which is a possible strategy to decrease CO₂ emissions into the atmosphere.^{6,7} At these depths, clathrate hydrates tend to form at the interface between the liquid CO₂ droplets and sea water. Their presence affects the mass transfer of the CO₂ and the hydrodynamics of the droplets. More specifically, physical properties of the clathrate hydrates, such as the diffusivity of H₂O and CO₂ within them, will determine the nature of the clathrate hydrates that form at the interface, and consequently the effect of the clathrate hydrate layer on the dispersion of CO₂ in the ocean.

Several experiments^{8–14} have been performed in which CO₂ drops were injected into water, and the formation of clathrate hydrate film around the CO₂ droplet was observed. None of the macroscopic models proposed to describe this process^{15–17} are able to provide a predictive and quantitative

estimate of the rate of dispersion of CO₂ in water, because there are too many unknown quantities in each of the models. Thus, in order to evaluate existing models and construct new ones, there is a need to obtain physical–chemical properties, such as rates of diffusion of CO₂ and H₂O in clathrate hydrates, independently of experiments involving the dissolution of CO₂ droplets.

No quantitative experimental or molecular modeling studies of the diffusion processes in clathrate hydrates have been performed up until now. Before this study, to the best of our knowledge, no one has proposed a mechanism for the diffusion of guest molecules and H₂O in clathrate hydrates, nor has anyone even estimated these diffusivities based on any properties of clathrate hydrates. In fact, in the literature, diffusivities in clathrate hydrates have been guessed by using diffusivities in polymer melts⁸ and in zeolites,⁹ both clearly very different materials from clathrate hydrates. On the other hand, the self-diffusion of H₂O in hexagonal ice has been studied quantitatively via experiments^{1–3} and qualitatively via molecular modeling simulations.⁴ In hexagonal ice, the migration of interstitial water molecules was shown to be the mechanism by which diffusion occurs.^{18,19} It was concluded that this mechanism dominates vacancy migration because of the low concentration of vacancies relative to that of interstitials.^{1,3}

In this work we have used classical inter-molecular potential models for H₂O and CO₂ to compute the diffusivities in ice and in CO₂ clathrate hydrates. The former was performed primarily in order to investigate the validity of these potentials for predicting diffusivities. Once this was accomplished, we then performed molecular dynamics and Monte Carlo simulations in order to calculate the self diffusion of both CO₂ and H₂O in clathrate hydrates.

^{a)}Author to whom correspondence should be addressed. Electronic mail: trout@mit.edu

II. THEORY AND METHODS

A. Potential models

Many effective pair potentials, such as TIP4P,²⁰ SPC,²¹ MCY,²² ST2,²³ SPC/E,²⁴ have been used for liquid water simulations. In our simulations, we decided to use the Extended Simple Point Charge (SPC/E) model, which predicts the self-diffusion coefficient of liquid water very well.^{24–26} The SPC/E model for water has a single Lennard-Jones (LJ) center representing the oxygen of the water molecule. In addition, the model has three partial charges: the negative charge is centered on the LJ center and two positive charges representing the hydrogens are placed such the H–O–H bond angle is 109.47°. When performing molecular dynamics simulations we constrain the two O–H bond lengths and the H–H distance within a single water molecule using the SHAKE (Ref. 29) algorithm. The parameters of the SPC/E model are optimized to reproduce the structure of liquid water at 300 K.²⁴ The SPC/E model is also shown to predict the self-diffusion coefficient of liquid water accurately.^{24–26} For modeling CO₂ molecules, we used the EPM2 potential model developed by Harris and Yung.²⁷ It has been shown that this model accurately predicts the vapor-liquid coexistence curve of pure CO₂ and the solubility of CO₂ in water.^{27,28} This model has three Lennard-Jones interaction sites with charges centered at each atom. When performing molecular dynamics simulations we leave the O–C–O angle flexible, with an angle potential of $\frac{1}{2}k_{\theta}(\theta - \theta_0)^2$, where θ_0 is 180°, and we constrain the C–O bond lengths using the SHAKE (Ref. 29) algorithm at a value of 1.149 Å. Parameters of interaction between the Lennard-Jones potential centers of CO₂ and H₂O molecules were calculated using the Lorentz–Berthelot combining rules.³⁰ Based on calculations performed by other authors,^{31,32} the melting temperature of SPC/E ice (without Ewald summation) was estimated to be 220 ± 20 K. Due to this limitation of the SPC/E model all our simulations were performed at 200 K. We also performed Monte Carlo simulations on the ice and the clathrate systems for the purpose of determining the free energy. The parameters of the inter molecular potentials used in the MC simulations were the same as that of the MD simulations described previously. However, for the sake of computational efficiency, the spring constants in the angle potential of CO₂ were made infinite, i.e., the CO₂ was treated as a rigid molecule. Owing to the rather large value of the energy parameter associated with the angle potential of CO₂ in the EPM2 model²⁷ compared to the simulation temperature of 200 K, the treatment of the CO₂ as a rigid molecule in the MC simulations is justified. In order to compute the free energies at higher temperatures (to enable comparison with experimental results at 273 K and compute desired properties at temperatures of interest), we used the internal energy and entropy computed at 200 K, and assumed that they are weak functions of temperature. For example, to compute the change in free energy $\Delta F^{(273\text{ K})}$, we used the following formula:

$$\Delta F^{(273\text{ K})} = \Delta U^{(200\text{ K})} - (273) \times \Delta S^{(200\text{ K})}. \quad (1)$$

TABLE I. Experimental self-diffusion coefficients of ice (Refs. 3 and 48). The diffusivities at 220 K, 253 K, and 263 K were reported directly in the references. The diffusivity at 200 K was extrapolated from these three values.

Temperature (K)	P (atm)	ρ (kg m ⁻³)	D_s (m ² s ⁻¹)
200	1	930.3	1.0×10^{-18}
220	1	927.4	1.8×10^{-17}
253	1	921.1	6×10^{-16}
263	1	918.3	1.5×10^{-15}

B. Details of simulations on hexagonal ice

An orthorhombic simulation supercell was chosen to study the hexagonal ice phase, with $a = b = 36.184$ Å and $c = 29.468$ Å. Molecular dynamics simulations were performed in the NVE ensemble using the CHARMM (Refs. 33–35) simulation package. There were a total of 1024 molecules in our system corresponding to a density of 0.030 68 molecules per Å⁻³. The density translates to a value of 916.8 kg m⁻³, which is close to the experimental density of ice at 273 K and 1 atm (see Table I). We note that the average density of SPC-E ice at 200 K and 1 atm determined using NPT Monte Carlo simulations was 916.8 kg m⁻³. The Verlet algorithm was used to propagate the system in time. A time step of 0.5 fs was used during equilibration and production runs. Periodic boundary conditions were applied in all three dimensions. The Ewald summation^{36,37} method was implemented with a κ value of 0.23 Å⁻¹, a cutoff radius of 14.73 Å (consistent with the minimum image convention) when performing the real-space summation, and the number of \mathbf{k} vectors $\approx 12^3$, to perform the summation in \mathbf{k} -space. The Ewald summation method was implemented using the Particle Mesh Ewald (PME) algorithm.³⁸

The positions of the oxygens in the hexagonal ice lattice obtained from x-ray diffraction data were used in the initial configuration of the MD simulation. The distribution of hydrogen atoms should satisfy several conditions: the protons should be rotationally disordered; hydrogen positions should satisfy ice rules referred to as *Bernal–Fowler rules*;^{39,40} and the net dipole moment of the ice structure should be equal to zero. We generated a number of proton disordered structures satisfying the ice rules using the method described by Buch *et al.*,⁴¹ and we calculated the net dipole moment of the whole structures. The configuration with the smallest dipole moment was picked for the subsequent simulations. We equilibrated the hexagonal ice structure for 20 ps at a simulation temperature of 200 K prior to collecting statistics. The total length of the MD simulation run was 0.5 ns.

C. Details of simulations on CO₂ clathrate hydrates

The simulation system consisted of 2 × 2 × 2 unit cells of the type I clathrate hydrate. Its dimensions were 24.06 × 24.06 × 24.06 Å; it contained 368 water molecules and 54 CO₂ molecules at a density of 0.0303 molecules per Å⁻³; and it was equilibrated at 200 K. For the fractional occupancies of clathrate hydrate cages, we used the experimental results obtained using neutral diffraction studies by Henning *et al.*⁴² They report that between 60%–80% of the small

cages are occupied, and more than 90% of the large cages are occupied at 263 K. In our calculations, we assume that 70% and 90% of small and large cages, respectively, are occupied by the CO₂ molecules. We started with a clathrate lattice of 100% occupancy and removed CO₂ molecules at random to get the desired occupancy. The resulting configuration was used to begin the equilibration prior to the MC/MD run.

The implementation of the MD algorithm for the CO₂ clathrate was the same as that of hexagonal ice. Periodic boundary conditions were applied in all three dimensions. However, smaller cutoff's for the intermolecular potentials (equal to half the box length) were used, consistent with the smaller size of the clathrate simulation cell. The Ewald summation^{36,37} method was implemented with a κ value of 0.23 Å⁻¹, a cutoff radius of 12.0 Å (consistent with the minimum image convention) when performing the real-space summation, and the number of \mathbf{k} vectors $\approx 12^3$, to perform the summation in \mathbf{k} -space. The Ewald summation method was implemented using the Particle Mesh Ewalds (PME) algorithm.³⁸ Molecular dynamics simulations for a total time of 1.0 ns were required to calculate the self-diffusion coefficient of a water molecule in the CO₂ clathrate. However, the data collected over a time scale of 1 ns proved to be insufficient to accurately determine the self-diffusion coefficient of the CO₂ molecules. Therefore we had to resort to additional Monte Carlo simulations combined with free energy calculations to determine the self-diffusion coefficient of the CO₂ molecules. The parameters of the inter molecular potentials used in the MC simulations were the same as that of the MD simulations described previously. However, for the sake of computational efficiency, the spring constants in the angle potential of CO₂ were made infinite, i.e., the CO₂ was treated as a rigid molecule. Owing to the rather large value of the energy parameter associated with the angle potential of CO₂ in the EPM2 model²⁷ compared to the simulation temperature of 200 K, the treatment of the CO₂ as a rigid molecule in the MC simulations is justified. Later, it will become apparent that the quantitative estimate of the self-diffusion coefficient of CO₂ in the clathrate is obtained solely on the basis of Monte Carlo results. Therefore, formally our calculation of the self-diffusion coefficient pertains to the rigid version of the EPM2 model. The Monte Carlo simulations were performed in the NVT ensemble starting from the same initial configurations as the MD simulations. Average properties were calculated by performing 40–100 million individual MC steps, each MC step consists of either a translation or a rotation of a randomly chosen molecule from the simulation cell. During each rotation step, three angles were chosen at random. A randomly chosen molecule was rotated successively along x , y , and z axes by the three randomly chosen angles respectively. The maximum displacement step and extent of rotation of the H₂O and CO₂ molecules were adjusted during the simulation run to yield an acceptance ratio of 50% and 33% of the attempted translations and rotations, respectively. A parallel version of our Monte Carlo program was used to run on 8 processors.

D. Free energy method

Hopping of CO₂ molecules between cages is a rare event. Therefore, in order to calculate the hopping rates of the CO₂ molecules, we employed the Landau free energy methodology within the MC simulations to calculate the free energy barrier for cage hopping. This method relies on the calculation of the Landau free energy as a function of an effective order parameter (or a reaction coordinate), Φ , via NVT simulations, and hence is a natural choice for our purpose. The Landau free energy is defined by,⁴³

$$\Lambda[\Phi] = -k_B T \ln(P[\Phi]) + \text{constant}, \quad (2)$$

where $P[\Phi]$ is the probability of observing the system having an order parameter value between Φ and $\Phi + \delta\Phi$. The Helmholtz free energy can be calculated by the numerical integration of the Landau Free energy function over the order parameter Φ ,

$$\exp(-\beta F) = \int d\Phi \exp(-\beta \Lambda[\Phi]). \quad (3)$$

We used umbrella sampling⁴⁴ in conjunction with the Landau free energy method to overcome the difficulty of collecting reliable statistics of the probability density function $P[\Phi]$. We divided the Φ parameter space into 8 overlapping regions covering the path corresponding to CO₂ hopping between two cages. Monte Carlo simulation runs of 36×10^6 steps, 12×10^6 of which were spent on the equilibration, were run in each of these 8 regions. 86% of the total number of Monte Carlo steps were spent on changing the coordinates of the H₂O molecules, and 14% on changing the coordinates of the CO₂ molecules. Also 60% and 40% of the total number of Monte Carlo steps were spent on rotational and translational motions of the molecules, respectively. The arbitrary constants in Eq. (2), were adjusted in each of the eight windows to make the Landau free energy surface continuous along the order-parameter coordinate.⁴⁵ The choice of our order-parameter is described below.

In our model system, we identified one of two adjacent cages that had no guest molecule. Simulation runs were performed both with and without water vacancy in the common face between these two cages. We calculated four different values for the CO₂ hopping rates in systems with water vacancies. The first corresponds to hopping from a small to a large cage through a pentagonal face, the second corresponds to hopping from a large to a small cage through the pentagonal face, the third corresponds to hopping from a large to a large cage through the pentagonal face, and the fourth corresponds to hopping from a large to a large cage through the hexagonal face. Note that, because we introduced a water vacancy into the system, the pentagonal face contained only 4 water molecules and the hexagonal face contained 5 water molecules. For the order parameter Φ in Eq. (2) we chose the distance to the plane passing through the pentagonal or hexagonal face common to both cages. This plane was determined using a linear least square fit to the oxygen atoms in the molecules in each face. We set the sign of Φ based on the cage in which the CO₂ molecule was originally present.

To estimate the hopping rates of CO₂ molecules between clathrate hydrate cages we used transition state theory (TST).⁴⁶ In using TST, the system is assumed to be in local thermodynamic equilibrium during the process of barrier hopping. The hopping rates can then be calculated using the equation,

$$k = \frac{k_B T}{h} \exp\left(-\frac{\Delta F}{k_B T}\right), \quad (4)$$

where ΔF is a free energy barrier calculated using Eq. (3), and the ratio $(k_B T)/h$ is the *frequency factor*. The free energy barrier at other temperatures were calculated using Eq. (1).

E. Calculation of defect concentrations

In our study, the concentration of water vacancies in clathrate hydrates is an important parameter. However, there are no experiments reporting estimates of this quantity. Therefore, to calculate this value we employed the method of thermodynamic integration.⁴⁷ In this method, we perform computer simulations of the system with potential energy of the form,

$$U(\lambda) = U_0 + \lambda(U_1 - U_0), \quad (5)$$

where U_0 is the potential energy of the reference system (an ideal clathrate lattice without defects) and U_1 is the potential energy of the system of interest (clathrate structure with one water vacancy). λ is a coupling parameter for which $\lambda=0$ corresponds to reference system and $\lambda=1$ corresponds to the system of interest. The free energy difference of the two systems is obtained using the equation,

$$\Delta F = \int_0^1 d\lambda \left\langle \frac{\partial U(\lambda)}{\partial \lambda} \right\rangle. \quad (6)$$

To calculate the free energy of formation of the water vacancy, we chose a molecule at random, and parameterized point charges and Lennard-Jones ϵ parameter as $q(\lambda) \rightarrow \lambda q$, and $\epsilon(\lambda) \rightarrow \lambda \epsilon$, so that the state with $\lambda=0$ corresponded to the system with a vacancy, and the state with $\lambda=1$ corresponded to the system without a vacancy. We then performed Monte Carlo simulations for 10 different λ values, and via numerical integration of Eq. (6), calculated the free energy of formation of the water vacancy. The concentration of vacancies was determined using the equation,³

$$c = \kappa \exp\left(-\frac{\Delta F}{k_B T}\right) = \kappa \exp\left(-\frac{E_f}{k_B T}\right) \exp\left(\frac{S_f}{k_B}\right), \quad (7)$$

where ΔF is the free energy of the formation of vacancy, E_f and S_f are the energy and entropy of the formation of vacancy. Equation (7) is derived from basic statistical mechanics by assuming a chemical equilibrium between defect and lattice species. For example, we treat the vacancy formation as a chemical reaction that takes the defect free lattice to a lattice with one vacancy with the removed molecules in the ideal gas phase. Similarly, an interstitial site is formed when a defect free lattice combines with a molecule from the ideal gas phase. The prefactor κ is the ratio of the number of possible places for the defect molecules to the total number

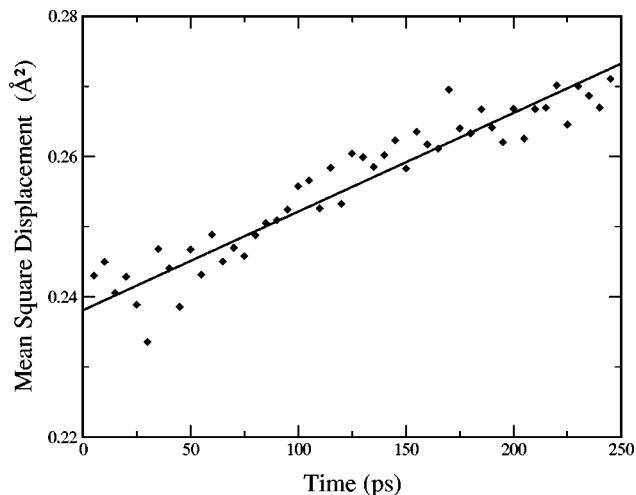


FIG. 1. Mean square displacement for the H₂O molecules in a hexagonal ice structure containing 1024 lattice water molecules and one interstitial water molecule. The MSD goes to zero at $t=0$ in the inertial regime which occurs within the first 5 ps. This is not shown in the plot which has a time resolution of 5 ps.

of lattice positions. For an interstitial type defect in ice, κ is 0.5, and for a vacancy in clathrate hydrate, κ is 1.

III. RESULTS AND DISCUSSIONS

A. Hexagonal ice

Molecular dynamics simulations of the ideal lattice of hexagonal ice for a 250 ps time period showed no evidence of diffusion. We then added one interstitial water molecule into the ideal lattice and simulated the ice structure containing 1024 water molecules at lattice positions and one interstitial molecule. We observed ~ 10 hoppings of interstitial water molecules during the 0.5 ns simulation run. The mean square displacement (MSD) of water molecules during this molecular dynamics run is plotted in Fig. 1. The slope of the line in Fig. 1 gives the diffusion coefficient associated with the interstitial molecule. To calculate the self-diffusion coefficient for the experimental system, we needed to account for the experimental concentration of interstitials. The concentration of interstitials reported in the experiment⁴⁸ is equal to 2.8×10^{-6} at 273 K. Using the experimental values of the energy and entropy of formation of the interstitial,³ 0.4 eV and $4.9 k_B$, respectively, and the following relation between the concentration of defects, c , the energy of formation of defects, E_f , and the entropy of formation, S_f :

$$c = \frac{1}{2} \exp\left(\frac{S_f}{k_B}\right) \exp\left(-\frac{E_f}{k_B T}\right), \quad (8)$$

we evaluated the concentration of interstitials at 200 K to be 5.6×10^{-9} . Note that the factor $\frac{1}{2}$ in Eq. (8) arises, because the number of interstitial sites in ice is half the number of molecular sites.⁴⁸

The slope of the curve in Fig. 1, determined using a linear square fit, is equal to $1.4 \times 10^{-12} \text{ m}^2 \text{ s}^{-1}$. Accounting for the concentration of interstitials and using the Einstein relation,

$$D = \lim_{t \rightarrow \infty} \frac{1}{6t} \langle |\mathbf{r}_i(t_0 + t) - \mathbf{r}_i(t_0)|^2 \rangle, \quad (9)$$

the self-diffusion coefficient is given by $c \times D$, and is calculated to be $1.3 \times 10^{-18} \text{ m}^2 \text{ s}^{-1}$ at 200 K. Hence, the self-diffusion coefficient is in good agreement with the experimental result given in Table I.

We also calculated the concentration of interstitials in hexagonal ice using Eq. (8) and the method described in Sec. II E. We estimated the entropy of formation of a water interstitial to be equal to $6.19 k_B$, and the energy of formation to be equal to 0.40 eV. These can be compared to the experimental values of $4.9 k_B$ and 0.4 eV respectively.³ Therefore, the computed concentration of water interstitials is equal to 9.0×10^{-6} at 273 K, compared to the experimental result³ of 2.8×10^{-6} at 273 K. In order to verify that the interstitial migration is the dominant mechanism for diffusion in ice, we calculated the free energy of formation of a vacancy in the ice lattice. Using the methodology in Sec. II E, we obtained a value of $2.34 k_B$ for the entropy of formation and 0.409 eV for the energy of formation of a water vacancy at 273 K. Therefore, using Eq. (7), the concentration of vacancies in ice at 273 K is equal to 2.88×10^{-7} . Since the concentration of vacancies in ice lower than that of water interstitials by a factor of 30, the diffusion mechanism in ice is dominated by the migration of interstitials. This is consistent with the experimental findings of Hondoh *et al.*¹⁻³

B. Clathrate hydrates

Molecular dynamics simulations of an ideal clathrate hydrate structure, with all small cages and 5% of the large cages containing no guest molecules, showed no evidence of diffusion. However, we were able to observe diffusion in the presence of a water vacancy. We introduced one water vacancy into the system with small cages containing no guest molecules and removed one CO₂ molecule from the large cage neighboring the water vacancy. After a simulation of 0.5 ns at a simulation temperature equal to 200 K, we observed the hopping of both H₂O and CO₂ molecules. We observed 4 hoppings of CO₂ molecules between large cages, which corresponds to a hopping rate of 8×10^9 hops/s. The mean square displacement plot of the H₂O molecules is shown in Fig. 2. Taking into account that our system contains 367 water molecules and one water vacancy, we calculated the diffusion coefficient of one water vacancy to be $5.1 \times 10^{-11} \text{ m}^2 \text{ s}^{-1}$ at 200 K. To determine the diffusivity of H₂O in clathrate hydrates we need to multiply the diffusion coefficient of one water vacancy by the concentration on water vacancies in clathrate hydrates. We report these numbers below.

Monte Carlo simulations of the system containing no water defects yielded a very high barrier for the hopping of the CO₂ molecules between cages. The free energy barrier for this process is shown in Fig. 3 where the two minima correspond to the CO₂ molecules being in the centers of the cages. We noticed that even though the system originally contained no water defects, a pair of water interstitial and water vacancy was spontaneously created to allow for CO₂ to hop to the neighboring cage. The estimate of the free

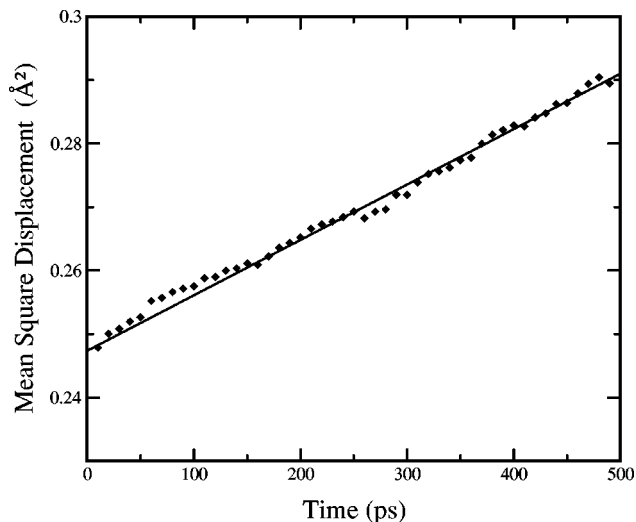


FIG. 2. Mean square displacement for the water molecules in a clathrate hydrate structure containing one water vacancy. The MSD goes to zero at $t=0$ in the inertial regime which occurs within the first 5 ps. This is not shown in the plot which has a time resolution of 5 ps.

energy barrier from Fig. 3 is $20.1 k_B T$ (0.3467 eV) at 200 K, with energy barrier equal to 0.36 eV. The free energy barrier [calculated using Eq. (1)] is equal to $14.4 k_B T$ (0.339 eV) at 273 K, which corresponds to a hopping rate of 3.2×10^6 hops/s, calculated using Eq. (4).

The free energy barrier for the hopping of CO₂ from a small to a large cage through a pentagonal face containing a water vacancy is shown in Fig. 4, where the value of the order parameter of 1 corresponds to a CO₂ molecule present at the center of a small cage, and the value of the order parameter of -1 corresponds to a CO₂ molecule present at the center of a large cage. The free energy barrier of hopping from a small to a large cage is estimated to be $5.7 k_B T$ (0.098 32 eV) at 200 K, and energy barrier is equal to 0.1 eV, and, therefore, the free energy barrier is equal to $4.14 k_B T$ (0.097 48 eV) at 273 K. The free energy barrier of hopping

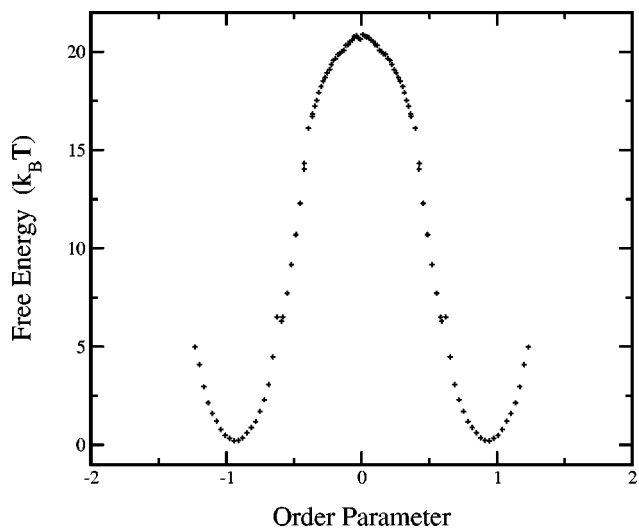


FIG. 3. Free energy barrier for the hopping of the CO₂ molecule between clathrate hydrate cages containing no water defects.

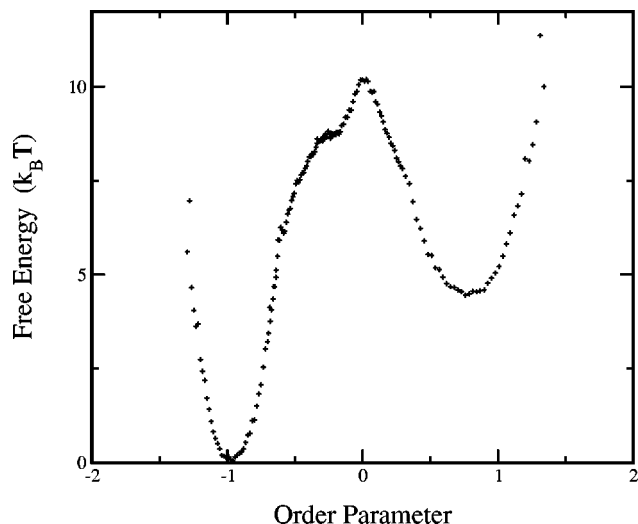


FIG. 4. Free energy barrier for the hopping of the CO₂ molecule between small and large clathrate hydrate cages with a water vacancy present between them.

from a large to a small cage is equal to $10.1 k_B T$ (0.1742 eV) at 200 K, the energy barrier is equal to 0.23 eV, and, therefore, the free energy barrier is equal to $6.46 k_B T$ (0.1521 eV) at 273 K. Using Eq. (4), we calculated the hopping rates from a large to a small and from a small to a large cages to be equal to 8.9×10^9 hops/s and 9.1×10^{10} hops/s, respectively. The free energy barrier for the hopping of CO₂ from a large to a large cage through a pentagonal face containing a water vacancy is shown in Fig. 5, and is equal to $6.6 k_B T$ (0.1138 eV) at 200 K. The energy barrier for the hopping is equal to 0.13 eV, and, therefore, the free energy barrier is equal to $4.5 k_B T$ (0.1059 eV) at 273 K. The corresponding hopping rate is equal to 6.2×10^{10} hops/s. Finally, the free energy barrier for the hopping of CO₂ from a large to an empty large cage through a hexagonal face containing a water vacancy is shown in Fig. 6, and is equal to $7.7 k_B T$ (0.1328 eV) at 200 K. Energy barrier for the hopping is equal

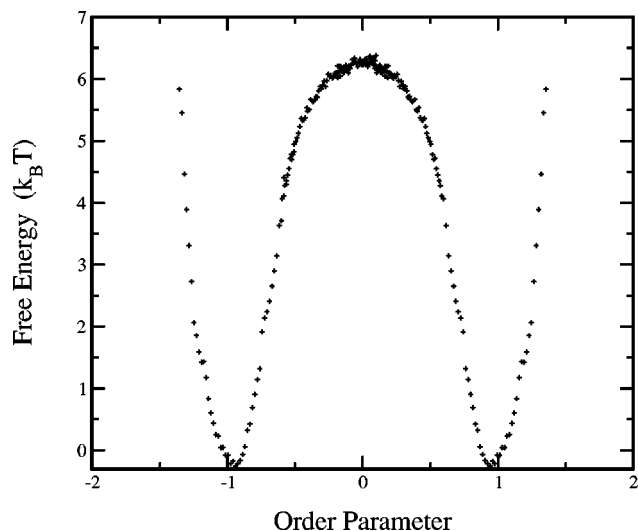


FIG. 5. Free energy barrier for the hopping of the CO₂ molecule between large and large clathrate hydrate cages through the pentagonal water face.

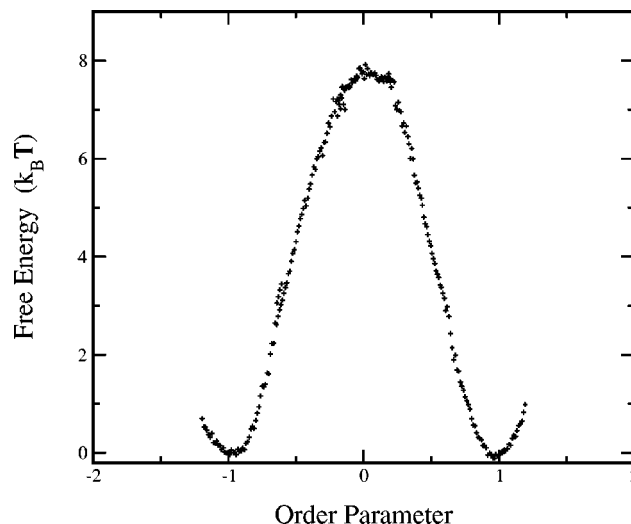


FIG. 6. Free energy barrier for the hopping of the CO₂ molecule between large and large clathrate hydrate cages through the hexagonal water face.

to 0.15 eV, and, therefore, the free energy barrier is equal to $5.3 k_B T$ (0.1248) at 273 K, and the corresponding hopping rate is equal to 2.8×10^{10} hops/s. A summary of the hopping rates is provided in Table II.

The largest hopping rate exists for the hopping of the CO₂ molecule from a large cage to a large cage with the vacancy present on the pentagonal water face. This hopping rate at 200 K is equal to 5.7×10^9 hops/s which is in a good agreement with the hopping rate of 8×10^9 hops/s at 200 K obtained through the molecular dynamics simulation.

To calculate the concentration of water vacancies in clathrate hydrates, we used the method described in Sec. II E. We justified the validity of using this method via the calculation of the concentration of interstitials in hexagonal ice (in that case we obtained the concentration of interstitials three times larger than the experimental results). We calculated the free energy of formation of water vacancies in clathrate hydrates to be 0.51 eV at 200 K (see Fig. 7), and the energy of formation of vacancies was calculated to be $E_f = 1.31$ eV. Therefore, the entropy of the formation of a water vacancy is equal to $46.42 k_B$, and the concentration of water vacancies determined, using Eq. (7), is equal to 1.0×10^{-4} at 273 K and 1.5×10^{-13} at 200 K.

Using the estimate of the concentration of water vacancies in CO₂ clathrate hydrates and the root mean square displacement of the water vacancies calculated via our molecular dynamics simulation, we estimated the diffusion coefficient of H₂O in clathrate hydrates to be $1 \times 10^{-23} \text{ m}^2 \text{ s}^{-1}$ at 200 K.

TABLE II. CO₂ hopping rates between clathrate hydrate cages with a water vacancy^a between them. Hopping rates were calculated via Monte Carlo simulations and correspond to a temperature of 273 K.

Large to large through pentagonal face	6.2×10^{10} hops/s
Large to large through hexagonal face	2.8×10^{10} hops/s
Small to large through pentagonal face	9.1×10^{10} hops/s
Large to small through pentagonal face	8.9×10^9 hops/s

^aThe hopping rate of CO₂ without water vacancy is 3.2×10^6 hops/s.

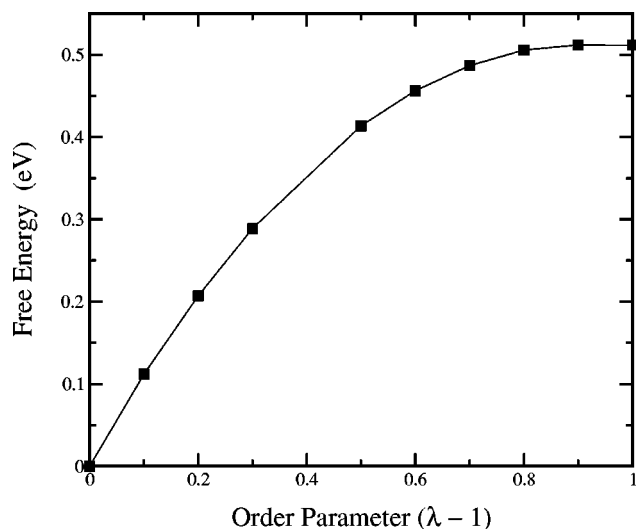


FIG. 7. Free energy of formation of a water vacancy in the clathrate hydrate structure.

An accurate calculation of the self-diffusion coefficient for CO_2 in hydrate involves the use of Eq. (9). However, as pointed out by Einstein,⁴⁹ a fairly accurate estimate of the diffusion coefficient, D , can be obtained using the expression $\frac{1}{6}\bar{d}^2/\bar{\tau}$, where \bar{d} is the length scale of the dominant molecular motion responsible for the diffusion and $\bar{\tau}$ is the time scale in which the dominant molecular motion occurs. Using the result that the diffusion of CO_2 occurs mainly through the hopping of the CO_2 molecule between large cages connected by the pentagonal water face containing one water vacancy, and assuming that the occupancy of the large cages is 90% we estimated the diffusion coefficient of CO_2 in the clathrate hydrate using formula,

$$D = \frac{1}{6} (d_{\text{cage-cage}}^2) \left(\frac{\text{hopping}}{\text{rate}} \right) \left(\frac{\text{connectivity}}{\text{of cages}} \right) \left(\frac{\text{occupancy}}{\text{of cages}} \right) \times \left(\frac{\text{concentration of}}{\text{water vacancies}} \right) \left(\frac{\text{H}_2\text{O molecules}}{\text{in the water face}} \right), \quad (10)$$

which leads to,

$$D_{ll5} = \frac{1}{6} \cdot 36 \times 10^{-20} \cdot 6.2 \times 10^{10} \cdot 8 \cdot 0.1 \cdot 1.0 \times 10^{-4} \cdot 5 = 1 \times 10^{-12} \text{ m}^2 \text{ s}^{-1}, \quad (11)$$

where 8 stands for the number of large cages adjacent to the large cage through the pentagonal face, 0.1 means that 10% of the large cages are empty, 1.0×10^{-4} is the concentration of water vacancies, and 5 is the number of water molecules in a pentagonal face. In Eq. (10), the last 4 terms adjust the hopping rate computed from our simulation to that of an experimental system at the desired conditions.

Using Eq. (10), we can estimate the diffusion coefficient corresponding to the diffusion from large to large cages through the hexagonal faces,

$$D_{ll6} = \frac{1}{6} \cdot 36 \times 10^{-20} \cdot 2.8 \times 10^{10} \cdot 2 \cdot 0.1 \cdot 1.0 \times 10^{-4} \cdot 6 = 2 \times 10^{-13} \text{ m}^2 \text{ s}^{-1}. \quad (12)$$

Another possible mechanism for the diffusion from large to large cages corresponds to a chain of hopping from a large to a small cage, followed by hopping from a small to a large cage. Diffusion corresponding to the first step in the chain is equal to

$$D_{ls} = \frac{1}{6} \cdot 36 \times 10^{-20} \cdot 8.9 \times 10^9 \cdot 4 \cdot 0.3 \cdot 1.0 \times 10^{-4} \cdot 5 = 3 \times 10^{-13} \text{ m}^2 \text{ s}^{-1}. \quad (13)$$

Diffusion corresponding to the second step in the chain, the hopping from a small to a large cage, is equal to

$$D_{sl} = \frac{1}{6} \cdot 36 \times 10^{-20} \cdot 9.1 \times 10^{10} \cdot 12 \cdot 0.1 \cdot 1.0 \times 10^{-4} \cdot 5 = 2 \times 10^{-11} \text{ m}^2 \text{ s}^{-1}. \quad (14)$$

Therefore, the total diffusion corresponding to the migration of the CO_2 molecules from large to large cages through small cages, calculated using the formula,

$$\frac{1}{D} = \frac{1}{D_1} + \frac{1}{D_2} \quad (15)$$

is equal to

$$D_{lsl} = 3 \times 10^{-13} \text{ m}^2 \text{ s}^{-1}. \quad (16)$$

Therefore, our original assumption that diffusion occurs mainly through the migration of the CO_2 molecules from large to large cages through pentagonal faces is accurate.

IV. CONCLUSIONS

Molecular simulation methods have been used to model the diffusion properties of CO_2 clathrate hydrates and ice. The self-diffusion coefficient of H_2O in ice was calculated to be $1.3 \times 10^{-18} \text{ m}^2 \text{ s}^{-1}$ at 200 K, in good agreement with experimental data. The concentration of water vacancies in the clathrate hydrate structure was estimated to be 1.0×10^{-4} at 273 K. The diffusion coefficient of CO_2 in CO_2 clathrate hydrates was estimated using Monte Carlo simulation techniques to be equal to $1 \times 10^{-12} \text{ m}^2 \text{ s}^{-1}$ at 273 K. The diffusivity of H_2O in the CO_2 clathrate hydrate is estimated to be equal to $1 \times 10^{-23} \text{ m}^2 \text{ s}^{-1}$ at 200 K, given that the concentration of water vacancies at 200 K is equal to 1.5×10^{-13} .

Possible future work includes a better estimation of the concentration of water vacancies in clathrate hydrates, and enhanced accuracy in the determination of the occupancies of clathrate cages. These two factors play very crucial role for the determination of the diffusion coefficient in CO_2 clathrate hydrates.

ACKNOWLEDGMENTS

The authors would like to acknowledge funding from the DOE Office of Science through the DOE Center for Research on Ocean Carbon Sequestration (DOCS).

¹T. Hondoh, T. Itoh, and A. Higashi, *Jpn. J. Appl. Phys.* **20**, L737 (1981).

²K. Goto, T. Hondoh, and A. Higashi, in *Point Defects and Defect Interactions in Metals*, edited by J. Takamura, M. Doyama, and A. Higashi (University of Tokyo Press, Tokyo, 1982), p. 174.

³K. Goto, T. Hondoh, and A. Higashi, *Jpn. J. Appl. Phys.* **25**, 351 (1986).

⁴H. Itoh, K. Kawamura, T. Hondoh, and S. Mae, *J. Chem. Phys.* **105**, 2408 (1996).

- ⁵E. D. Sloan, *Clathrate Hydrates of Natural Gases* (Dekker, New York, 1990).
- ⁶C. Marchetti, *Climatic Change* **1**, 59 (1977).
- ⁷M. Steinberg, *An Analysis of Concepts for Controlling Atmospheric Carbon Dioxide, DOE/CH/00016-1* (Brookhaven National Laboratory, Brookhaven, NY, 1984).
- ⁸R. P. Warzinski, P. D. Bergman, S. P. Masutani, and G. D. Holder, *A. Chem. Soc., Div. Fuel. Chem.* **42**, 578 (1997) (preprint).
- ⁹K. Ogaswara, A. Yamasaki, and H. Teng, *Energy Fuels* **15**, 147 (2001).
- ¹⁰I. Aya, K. Yamane, and N. Yamada, in *Fundamentals of Phase Change: Freezing, Melting, and Sublimation*, Vol. 215 in *HTD*, edited by P. E. Kroeger and Y. Bayazitoglu (The American Society of Mechanical Engineers, Fairfield, NJ, 1992), p. 17.
- ¹¹H. Kimuro *et al.*, *Energy Convers. Manage.* **34**, 1089 (1993).
- ¹²H. Kimuro *et al.*, *IEEE Trans. Energy Conversion* **9**, 732 (1994).
- ¹³Y. Fujioka, K. Takeuchi, Y. Shindo, and H. Komiyama, *Int. J. Energy Res.* **18**, 765 (1994).
- ¹⁴S. Hirai *et al.*, *Energy Convers. Manage.* **36**, 471 (1995).
- ¹⁵S. Hirai *et al.*, *Energy Convers. Manage.* **37**, 1073 (1996).
- ¹⁶Y. Mori and T. Mochizuki, *Chem. Eng. Sci.* **52**, 3613 (1998).
- ¹⁷Y. Mori, *Energy Convers. Manage.* **39**, 1537 (1998).
- ¹⁸K. Itagaki, *J. Phys. Soc. Jpn.* **22**, 427 (1967).
- ¹⁹R. O. Ramseyer, *J. Appl. Phys.* **38**, 2553 (1967).
- ²⁰W. L. Jorgensen *et al.*, *J. Chem. Phys.* **79**, 926 (1983).
- ²¹H. J. C. Berendsen, J. P. M. Postma, W. F. van Gunsteren, and J. Hermans, in *Intermolecular Forces*, edited by B. Pullman (Reidel, Dordrecht, 1981), p. 331.
- ²²O. Matsuoka, E. Clementi, and M. Yoshimine, *J. Chem. Phys.* **64**, 1351 (1976).
- ²³F. H. Stillinger and A. Rahman, *J. Chem. Phys.* **60**, 1545 (1974).
- ²⁴H. J. C. Berendsen, J. R. Grigera, and T. P. Straatsma, *J. Phys. Chem.* **91**, 6269 (1987).
- ²⁵L. A. Báez and P. Clancy, *J. Chem. Phys.* **103**, 9744 (1995).
- ²⁶L. A. Báez and P. Clancy, *J. Chem. Phys.* **101**, 9837 (1994).
- ²⁷J. G. Harris and K. H. Yung, *J. Phys. Chem.* **99**, 12021 (1995).
- ²⁸J. R. Errington, K. Kiyohara, K. E. Gubbins, and A. Z. Panagiotopoulos, *Fluid Phase Equilib.* **151**, 33 (1998).
- ²⁹J. P. Ryckaert, G. Ciccotti, and H. J. C. Berendsen, *J. Comput. Phys.* **23**, 327 (1977).
- ³⁰M. P. Allen and D. J. Tildesley, *Computer Simulation of Liquids* (Oxford University Press, Oxford, 1987).
- ³¹G. T. Gao, X. C. Zeng, and H. Tanaka, *J. Chem. Phys.* **112**, 8534 (2000).
- ³²O. A. Karim and A. D. J. Haymet, *Chem. Phys. Lett.* **138**, 531 (1987).
- ³³B. R. Brooks *et al.*, *J. Comput. Chem.* **4**, 187 (1983).
- ³⁴A. MacKerrell, Jr. *et al.*, *J. Phys. Chem. B* **102**, 3586 (1998).
- ³⁵E. Neria, S. Fischer, and M. Karplus, *J. Chem. Phys.* **105**, 1902 (1996).
- ³⁶P. P. Ewald, *Ann. Phys. (Leipzig)* **54**, 519 (1917a).
- ³⁷P. P. Ewald, *Ann. Phys. (Leipzig)* **64**, 253 (1921).
- ³⁸U. Essmann *et al.*, *J. Chem. Phys.* **103**, 8577 (1995).
- ³⁹J. D. Bernal and R. H. Fowler, *J. Chem. Phys.* **1**, 515 (1933).
- ⁴⁰P. V. Hobbs, *Ice Physics* (Clarendon, Oxford, 1974).
- ⁴¹V. Buch, P. Sandler, and J. Sadlej, *J. Phys. Chem. B* **102**, 8641 (1998).
- ⁴²R. W. Henning, A. J. Schultz, V. Thieu, and Y. Halpern, *J. Phys. Chem. A* **104**, 5066 (2000).
- ⁴³L. D. Landau and E. M. Lifshitz, *Statistical Physics*, 3rd ed. (Pergamon, London, 1980).
- ⁴⁴G. M. Torrie and J. P. Valleau, *J. Comput. Phys.* **23**, 187 (1977).
- ⁴⁵R. Radhakrishnan and K. E. Gubbins, *Mol. Phys.* **96**, 1249 (1999).
- ⁴⁶J. I. Steinfeld, J. S. Francisco, and W. L. Hase, *Chemical Kinetics and Dynamics* (Prentice-Hall, Upper Saddle River, NJ, 1998).
- ⁴⁷D. Frenkel and A. J. C. Ladd, *J. Chem. Phys.* **81**, 3188 (1984).
- ⁴⁸V. F. Petrenko and R. W. Whitworth, *Physics of Ice* (Oxford University Press, Oxford, 1999).
- ⁴⁹A. Einstein, *Investigations on the Theory of Brownian Movement* (Dover, New York, 1956).